Tuning the antiferromagnetic helical pitch length and nanoscale domain size in Fe_{3}PO_{4}O_{3} by magnetic dilution

M. J. Tarne, M. M. Bordelon, S. Calder, J. R. Neilson, and K. A. Ross

Tuning the antiferromagnetic helical pitch length and nanoscale domain size in $Fe_3PO_4O_3$ by magnetic dilution

Tarne, M.J.,[1] Bordelon, M.M.,[1] Calder, S.,[2] Neilson, J.R.,[1] and Ross, K.A.[3, *]

[1]*Department of Chemistry, Colorado State University, Fort Collins, Colorado 80523, USA*
[2]*Quantum Condensed Matter Division, Oak Ridge National Laboratory, Oak Ridge, Tennessee 37831, USA*
[3]*Department of Physics, Colorado State University, Fort Collins, Colorado 80523, USA*

The insulating magnetic material $Fe_3PO_4O_3$ features a non-centrosymmetric lattice composed of Fe^{3+} triangular units. Frustration, due to competing near neighbor (J_1) and next nearest neighbor (J_2) antiferromagnetic interactions, was recently suggested to be the origin of an antiferromagnetic helical ground state with unusual needle-like nanoscale magnetic domains in $Fe_3PO_4O_3$. Magnetic dilution is shown here to tune the ratio of these magnetic interactions, thus providing deeper insight into this unconventional antiferromagnet. Dilution of the Fe^{3+} lattice in $Fe_3PO_4O_3$ was accomplished by substituting non-magnetic Ga^{3+} to form the solid solution series $Fe_{3-x}Ga_xPO_4O_3$ with $x = 0.012, 0.06, 0.25, 0.5, 1.0, 1.5$. Magnetic susceptibility and neutron powder diffraction data from this series are presented. A continuous decrease of the both the helical pitch length and the domain size is observed with increasing dilution up to at least $x = 0.25$, while for $x \geq 0.5$, the compounds lack long range magnetic order entirely. The decrease in the helical pitch length with increasing x can be qualitatively understood by reduction of the ratio of J_2/J_1 in the Heisenberg model, consistent with mean field considerations. Intriguingly, the magnetic correlation length in the ab plane remains nearly equal to the pitch length for each value of $x \leq 0.25$, showing that the two quantities are intrinsically connected in this unusual antiferromagnet.

I. INTRODUCTION

Magnetic frustration, arising from competing interactions, can lead to a variety of interesting phenomena. The roster of frustration-induced effects includes noncollinear spin structures[1,2], spin glasses[3], multiferroics[4], and spin liquids[5]. In each case, the delicate balance of interactions means that small perturbations, such as magnetic dilution, can lead to dramatic effects.

When frustration leads to helical magnetic structures, the possibility of interesting topological defects such as vortices, magnetic bubbles, or Skyrmions arises[6]. Skyrmions in particular are of current interest for their possible uses in spintronics applications[7]. The Skyrmion lattice phase known for the B20 compounds, which display a competition between ferromagnetic (FM) Heisenberg and Dzyaloshinksii-Moriya (DM) interactions, can be thought of as a combination of helical orders resulting in a multi-k incommensurate structure, which emerges from a helical parent phase under the application of a magnetic field[8,9]. In the same vein, it is also possible to nucleate single Skrymions at the intersection of helical domain walls[10,11]. Therefore, one may also expect the magnetic domain walls in helical magnets to be interesting topological defects in their own right.

Locally antiferromagnetic (AFM) helical order, which resembles AFM order at short length scales, is less commonly observed than locally FM helical order. This type of order produces the telltale signature in neutron scattering experiments of satellite Bragg peaks surrounding commensurate AFM zone centers. A magnetic structure like this has been recently studied in the insulating Fe^{3+}-based material $Fe_3PO_4O_3$[12]. However, in this material the satellite peaks are significantly broadened in two out of three dimensions, implying the presence of nanoscale needle-like domains of AFM helical order. This, in turn, implies a high density of topological defects, and whether theses are domain walls, or possibly more exotic structures such as AFM Skyrmions[11,13,14], remains to be determined. In this report, we shed new light on this unusual magnetic structure and its defects by diluting the magnetic lattice, revealing that the planar correlation length is intrinsically linked to the helical pitch length.

The structure of $Fe_3PO_4O_3$ (noncentrosymmetric space group $R3m$ with room temperature lattice parameters of $a = b = 8.006$ Å and $c = 6.863$ Å in the hexagonal setting) can be described as triangular units of distorted FeO_5 trigonal bipyramids coordinated by phosphate groups as shown in Figure 1a. Figures 1b and c show the connectivity of magnetic Fe^{3+} cations; J_1 nearest-neighbor interactions are shown in blue within the triangles and J_2 next-nearest-neighbor interactions are shown in orange between neighboring triangles. When these interactions are AFM and isotropic (as expected in $Fe_3PO_4O_3$ based on the lack of single-ion anisotropy expected for $S = \frac{5}{2}$ Fe^{3+} and significant direct exchange interactions[15]), this model produces helical magnetic states near the frustrated point $J_2/J_1 \approx 2$. Magnetization[15,16], specific heat[17], Mössbauer spectroscopy[15,16], and neutron powder diffraction[12,15] all confirm that $Fe_3PO_4O_3$ orders into an AFM structure below $T_N = 163$ K. The magnetic structure of $Fe_3PO_4O_3$ was recently shown to be quite unusual, however, in that the AFM helical state (Figure 1 d) is only partially ordered; the correlation length of the magnetic order extends to at least 90 nm (900 Å) along the c axis, but remains limited to $\xi_{ab} < 10$ nm in the ab plane down to at least $T = 4$ K[12].
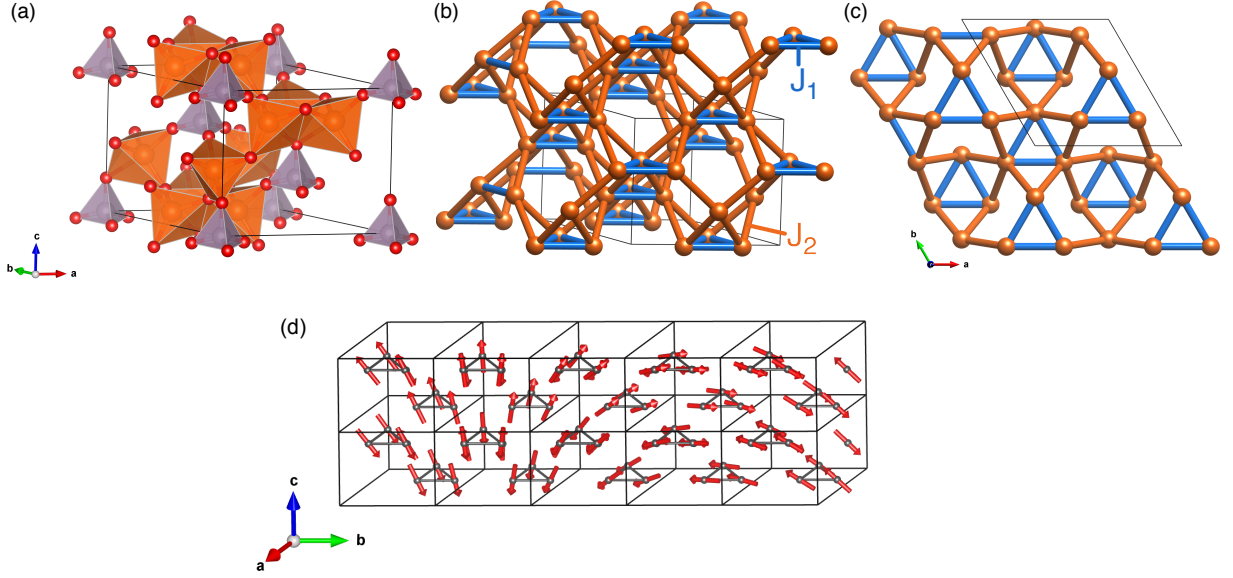
In this contribution we examine the magnetic order

FIG. 1. a) Crystal structure of $Fe_3PO_4O_3$. Iron is shown in orange, phosphorus in purple, and oxygen in red. b) Fe-Fe magnetic interactions in $Fe_3PO_4O_3$. J_1 bonds are shown in blue, J_2 bonds are shown in orange. c) View along the c axis, highlighting the triangular Fe^{3+} units in $Fe_3PO_4O_3$. d) Antiferromagnetic helical structure for the parent compound, $Fe_3PO_4O_3$. As the magnetic sublattice is diluted (increasing x in $Fe_{3-x}Ga_xPO_4O_3$), the same type of structure persists, but the helical pitch length and ab plane correlation length decrease in tandem.

in gallium-doped $Fe_{3-x}Ga_xPO_4O_3$ via low temperature magnetic susceptibility and neutron powder diffraction. We use the helical magnetic structure that was previously proposed[12] (Fig. 1 d) to model the neutron powder diffraction patterns of the gallium-substituted materials. For low dilution, $0 \leq x \leq 0.25$, the helical pitch length decreases with increasing x, which can be reproduced us-

ing a reduced ratio of J_2/J_1 in the Heisenberg exchange model. This is consistent with a mean field picture, since twice as many J_2 interactions are removed as compared to J_1 interactions for every Fe atom that is replaced with non-magnetic Ga. The size of the magnetic domains in the ab plane, determined via the broadening of magnetic Bragg peaks, is also reduced with increasing x. Curiously, the correlation length in the ab plane (equal to half of the typical domain size) appears to be constrained to be equal to the pitch length. At higher values of gallium substitution, $x \geq 0.5$, long-range magnetic order in any direction is not observed, providing an estimate for the percolation threshold for this lattice.

II. METHODS

Polycrystalline samples in the solid solution series $Fe_{3-x}Ga_xPO_4O_3$ were prepared as previously described[12]. Fe_2O_3 and Ga_2O_3 were dried overnight at $600°C$ and $FePO_4 \cdot nH_2O$ was converted to anhydrous $FePO_4$ by heating in air at $900°C$ overnight in alumina crucibles, and then stored in a desiccator. Powder X-ray diffraction data were collected using a NaCl internal standard to check for purity and for shifts in the lattice parameter. Data were collected using a Bruker D8 Discover DaVinci Powder X-ray Diffractometer. Rietveld refinements including explicit modeling of the NaCl standard were performed using the TOPAS software package. The refinements confirm a solid-solution behavior of $Fe_{3-x}Ga_xPO_4O_3$. The extracted lattice parameters fol-
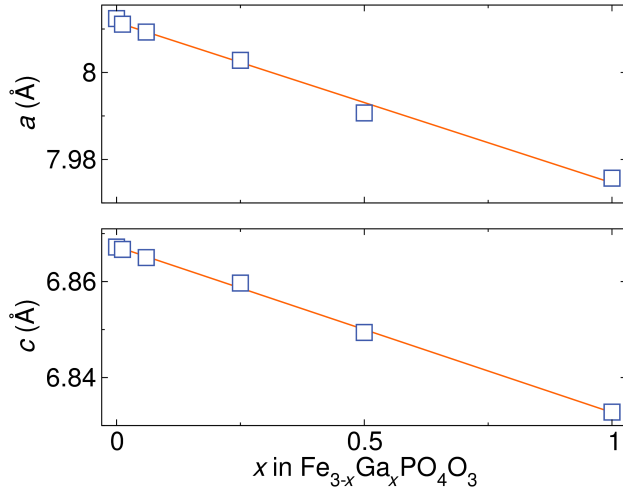

FIG. 2. Extracted lattice parameters, a (top panel) and c (bottom panel) from Rietveld refinements against room-temperature laboratory X-ray diffraction data, collected using NaCl as an internal standard. The orange lines are the interpolation between the previously reported values for $Fe_3PO_4O_3$[12] and $Ga_3PO_4O_3$[18].
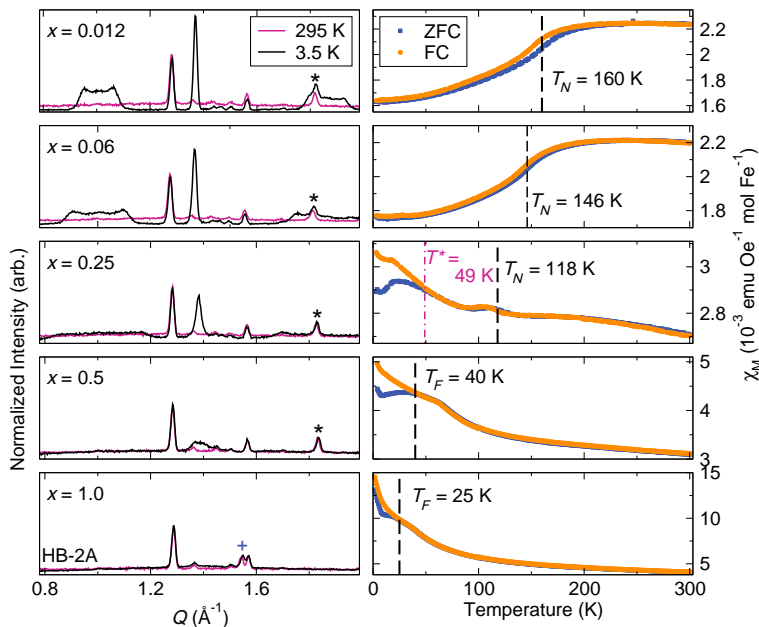
FIG. 3. Neutron powder diffraction (left) and magnetic susceptibility (right) for $x = 0.012$, 0.06, 0.25, 0.5, and 1.0 in $Fe_{3-x}Ga_xPO_4O_3$. The magnetic Bragg reflections centered at $Q = 1$, 1.35, 1.75 Å^{-1} decrease in intensity and broaden as gallium content increases. The magnetic susceptibility shows a decrease in the magnetic transition temperature with increased gallium substitution and eventually the development of a ZFC/FC splitting suggestive of a spin-frozen state. Although LRO order exists in $x = 0.25$ at 118 K, there is a lower temperature transition at 49 K denoted as T^* that does not correspond to changes in the static properties of the magnetic order. Small quantities of $FePO_4$ impurities in the NPD data are shown as black stars and $GaPO_4$ impurities as blue addition signs.

low Vegard's law for a solid solution between $Fe_3PO_4O_3$ and $Ga_3PO_4O_3$; the observed lattice parameters agree well with the extrapolated lattice parameters for a given value of x, suggesting that the actual composition reflects the nominal composition (Figure 2).

Magnetization measurements were performed using a vibrating sample magnetometer in a Quantum Design Physical Properties Measurement System. The samples were measured in an applied field of $\mu_0 H = 1$ T from $T = 1.8$ K to 300 K after cooling in the absence of an applied magnetic field (zero field cooled measurement, a.k.a. ZFC), and then measured from 300 to 1.8 K in a 1T field (field cooled measurement, a.k.a. FC).

Neutron powder diffraction (NPD) measurements were carried out on 2.3-2.6 g polycrystalline samples of $Fe_{3-x}Ga_xPO_4O_3$ with $x = 0$, 0.012, 0.06, 0.25, 0.5, 1.0, and 1.5 using beamline HB-2A at the High Flux Isotope Reactor at Oak Ridge National Laboratory. The samples were measured at temperatures ranging from 3.5 to 295 K using a helium closed cycle refrigerator; collection temperatures were selected based on features observed in susceptibility measurements. The instrument provided a constant wavelength incident neutron beam with $\lambda = 2.4123$ Å from the Ge(113) monochromator, and 21 arcminute collimators were placed between the monochromator and the sample, while 12 arcminute collimators

were used between the sample and each of the 44 detectors. This configuration produces a resolution of $\Delta Q/Q = 1.5 \times 10^{-2}$ at $Q = 1$ Å^{-1}.[19] Magnetic and nuclear Rietveld refinements were performed using the FullProf software package[20].

Magnetic structures were determined for the classical $J_1 - J_2$ Heisenberg Hamiltonian for various ratios of J_2/J_1 using a numerical energy minimization routine implemented in the program SpinW (a simplex method with periodic boundary conditions)[21].

III. RESULTS

The low-temperature magnetic susceptibility as well as neutron diffraction patterns at high and low temperatures is shown in Figure 3 for all $x > 0$. A slight splitting between the FC and ZFC curves in the parent compound ($x = 0$, shown in Ref. 12) begins slightly above T_N and persists down to at least 2 K. Similar features are observed for $x = 0.012$ and $x = 0.06$ (Fig. 3), although T_N decreases with increasing x. T_N is estimated at 160 K for $x = 0.012$ and 146 K for $x = 0.06$, based on the location of the the largest positive dM/dT in the ZFC susceptibility, a feature which is coincident with a peak in the specific heat for $x = 0$ as shown in Ref. 12.
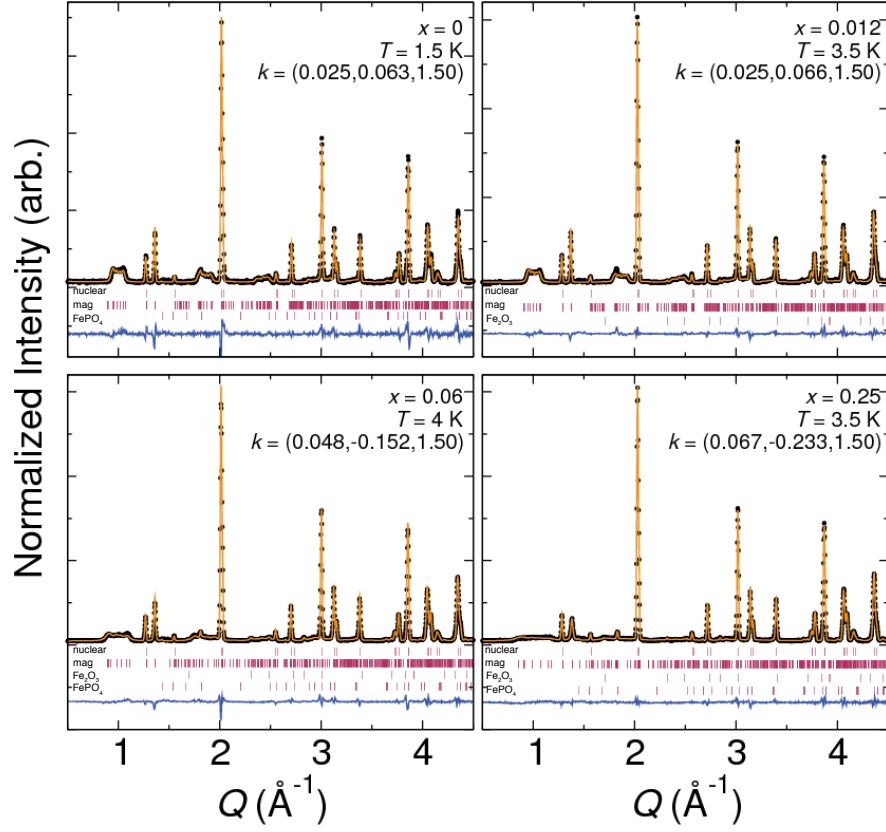
FIG. 4. Rietveld refinements using the Fullprof software package for the magnetically ordered members of the series $Fe_{3-x}Ga_xPO_4O_3$. The data are shown as black points, the fit is in orange, and tick marks show the central peak positions of nuclear, magnetic, and impurity phases. The difference curve is in blue.

A more dramatic ZFC/FC splitting occurs for $x > 0.06$. Based on comparison to the temperature dependent neutron powder diffraction patterns (Appendix, Fig. 7), discussed next, this splitting occurs at the temperature T^* which is *below* T_N for $x = 0.25$, possibly indicating a freezing of "free spins" produced by dilution (i.e., spins which are liberated from strong constraints on their orientation due to missing neighbors, also known as "orphan spins"[22]). For $x > 0.5$, a long-range ordered state is not observed, and the ZFC/FC splitting in the susceptibility might signal spin freezing throughout the entire sample, as in a spin glass. Accordingly, the temperature of the ZFC/FC splitting is denoted as T_F for $x > 0.5$. The overall magnitude of the susceptibility increases for $x > 0.5$, consistent with moving toward the paramagnetic limit as dilution acts to suppress the strong AFM correlations known to be present even up to 900 K in $Fe_3PO_4O_3$[12].

The magnetic structures for $x > 0$ remain qualitatively similar to the parent compound, as confirmed by NPD (Figure 4), although T_N decreases with gallium substitution as expected for overall weaker interactions produced by dilution[23,24]. The eventual disappearance of long-range order, which we characterize by absence of a well-formed magnetic peak near $Q=1.35$ Å^{-1}, occurs for $x \geq 0.5$.

The helical magnetic structure model previously used for the parent compound, with an ordering wavevector $\mathbf{k}_h = (\delta_a, \delta_b, 1.5)$ (hexagonal setting of $R3m$) and needle-like finite size broadening indicating a magnetic domain size in the ab plane, was fit to the data for $x \leq 0.25$ (Figure 4). The magnitude of this incommensuration, $|\delta| = \sqrt{(\delta_a + \frac{1}{2}\delta_b)^2 + (\frac{\sqrt{3}}{2}\delta_b)^2}$, increases with x, implying a reduced helical pitch length $l = \frac{a}{|\delta|}$ as shown in Figure 5b. The incommensuration is constant in temperature below T_N for each sample. For $x = 0.5$ at $T = 3.5$ K, the broad magnetic peaks are not visible and the normally sharp $(\delta_a, \delta_b, 3/2)$ peak near $Q \sim 1.35$ Å^{-1} is significantly broadened. For samples with $x \geq 1.0$, there are no magnetic Bragg features except for diffuse scattering centered at $Q \sim 1.35$ Å^{-1} as shown in Figures 3 and 5.

Correlation lengths can be extracted from the magnitude of the peak broadening required to match the slopes of the edges of the broad magnetic features. The coexistence of a sharp, resolution limited magnetic Bragg peak (near $Q \sim 1.35$ Å^{-1}) and broad, flat topped peaks (such as that near $Q \sim 1$ Å^{-1}) can be described by anisotropic broadening, which affects peaks that have large $\vec{Q}$ components in the ab plane (i.e., produced by needle-shaped domains). The Lorentzian broadening employed in the
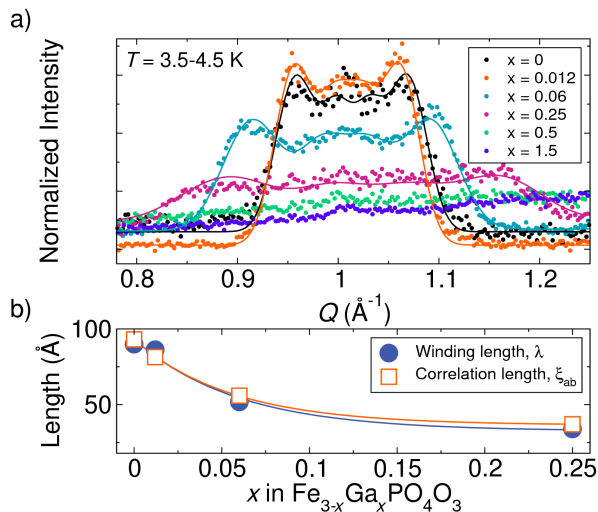
FIG. 5. a) Broad magnetic peak measured by NPD for different gallium concentrations in $Fe_{3-x}Ga_xPO_4O_3$ at $T = 3.5$ - 4.5 K; data is shown as points and the profile-matched fits are solid lines (see main text). The broad, flat-topped magnetic Bragg peak broadens and decreases in intensity with increased gallium content, consistent with a decrease in J_2 mean-field interaction strength relative to J_1. b) The helical winding length and ab plane magnetic correlation length are shown in the bottom panel as a function of gallium content; both decrease with gallium substitution and track each other. Error bars are smaller than the symbols. Solid lines added to guide the eye.

Fullprof Rietveld refinement software package does not accurately capture the shape of the broad peaks, particularly the slopes of the peak edges. In order to extract the ab-plane correlation length more accurately, we used a custom-made analysis script which fits the broad peak near 1 Å^{-1} and the sharp peak near 1.35 Å^{-1} simultaneously, applying a Gaussian broadening beyond the instrument resolution to the former, but not the latter. For this analysis, the peak locations were set by a single magnetic propagation vector, but intensities were permitted to refine independently (i.e., a LeBail, also known as profile-matching, pattern refinement method was used). This method allows us to refine the ordering wavevector, which is strongly constrained by the central Q of the sharp peak, and the correlation length ξ_{ab} simultaneously. The fits are shown in Figure 5, while the fits to the whole NPD pattern obtained using Lorentzian broadening as implemented in Fullprof are shown in Figure 4. The correlation length is extracted as $\xi_{ab} = \pi/\beta$, where β is the full width at half maximum (FWHM) of the satellite peaks with Q being the independent variable (the correlation length is taken to be the radius of the Scherrer domain size, assuming a shape factor of K = 1[25]). The ab plane correlation length decreases with increasing x, and remains approximately equal to the helical pitch length for all values of x (Figure 5). The marked increase in domain wall density (from $\frac{1}{\pi\xi_{ab}^2} = 0.0037$ nm^{-2}

at $x = 0$ to 0.023 nm^{-2} at $x = 0.25$) shows that magnetic dilution greatly stabilizes the formation of domain walls. Furthermore, the domain wall density is not consistent with a simple picture of nucleation at the gallium defects; assuming an even distribution of the defects, and taking $\frac{x}{3} \times 9$ Ga atoms per 55.5 Å^2 (there are 9 sites in the unit cell, which has an ab plane area of 55.5 Å^2), gives a domain wall density of 1.3 nm^{-2} at $x = 0.25$, which is much larger than observed.

IV. DISCUSSION

The magnetic frustration in $Fe_3PO_4O_3$ stems from the competition between the antiferromagnetic intra-triangle J_1 and inter-triangle J_2 interactions. As non-magnetic gallium substitutes into the structure, the magnetic J_2 and J_1 interactions are disrupted. For each gallium atom, two J_1 bonds and four J_2 bonds are broken, from which we expect a reduction in the average ratio J_2/J_1. The effect of this rebalancing of the exchange interactions was examined using a numerical minimization of the classical spin Hamiltonian,

$$\mathcal{H} = \sum_{<i,j>} J_1\mathbf{S}_i \cdot \mathbf{S}_j + \sum_{<<i,j>>} J_2\mathbf{S}_i \cdot \mathbf{S}_j \qquad (1)$$

where the first sum is over nearest neighbors and the second is over next nearest neighbors.

Planar helical magnetic structures with the $\mathbf{k}_h = (\delta_a, \delta_b, 1.5)$ ordering wavevector are produced when $J_2/J_1 \approx 2$. The ratio of J_2/J_1 was varied slightly, and the resulting helical modulation ($|k_{ab}| = \frac{2\pi}{a}|\delta|$) was determined. The variation in the helical pitch of the magnetic structure agrees qualitatively with the experimental results: $|k_{ab}|$ increases with decreasing J_2/J_1, as shown in Figure 6. Matching the calculated $|k_{ab}|$ to that of the parent compound ($|k_{ab}| = 0.073$ Å^{-1}), this approximation gives $J_2/J_1 = 1.96$ for $x = 0$ which is reduced to $J_2/J_1 = 1.84$ for $x = 0.25$, indicating that the mean J_2 interaction strength is reduced relative to J_1, as expected.

Some simplifying assumptions were made in the choice of the magnetic structure, as well as the Heisenberg model, discussed above. To within the constraints of our powder averaged neutron diffraction data, we cannot distinguish between coplanar (helical) versus some non-coplanar (conical) magnetic structures, as discussed in Ref. 12; we thus chose the former for simplicity. Furthermore, the crystal structure lacks any inversion center, implying the presence of Dzyaloshinskii-Moriya (DM) interactions for every pair of Fe atoms, which may favor non-coplanar conical structures. However, the simple model presented here captures the main features of the NPD of $Fe_3PO_4O_3$ and its variation with magnetic dilution; the pitch length and correlation length would not depend on the choice of a helical vs. conical structure, and although the mapping of $|k_{ab}|$ to the ratio of J_2/J_1 might be modified by the inclusion of DM interactions,
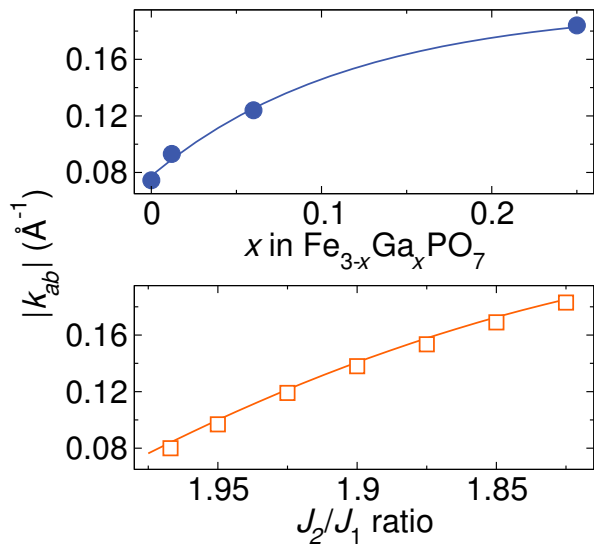
FIG. 6. Experimental (top) and calculated (bottom) values of the length of the magnetic propagation vector in the ab plane, $|k_{ab}|$, for Ga-doped $Fe_3PO_4O_3$. The mean-field model of decreased J_2/J_1 ratio with increased gallium substitution is consistent with experimental results. Lines added to guide the eye.

values of x below the percolation limit ($x \sim 0.5$). Since the decrease in the winding length can be understood as a decrease in J_2/J_1, an intrinsic effect, the connection between the domain size and the pitch length intriguingly suggests that helical domains are truncated due to an intrinsic instability of the helical structure toward defect formation. We note that the same relationship between helical pitch length and Skyrmion size is expected, since the Skyrmion size equals the helical pitch length of the parent phase. This observation, along with the motivation to discover and study AFM Skrymions in a real material, may provide the impetus to examine the magnetic defects in $FePO_4O_3$. This may be tackled experimentally or through simulations. The major challenge experimentally is that the net moment is expected to be zero, making standard probes of real space spin textures such as Lorentz transmission electron microscopy potentially intractable.

we expect this to be a small effect since the DM interactions arise from spin orbit coupling, which is weak for Fe^{3+}.

We note that the intensity distribution of the broad peaks are more symmetric than expected, since the Fe^{3+} magnetic form factor should tend to suppress the intensity at the high Q side. This disagreement becomes even more pronounced with the significantly broader peaks such as those in $Fe_{2.75}Ga_{0.25}PO_4O_3$. The inferred covalency of the Fe-O bonds in $Fe_3PO_4O_3$, discussed in Ref. 12, would produce a less localized spin distribution, weakening the magnetic form factor. Note that the profile-matching calculation shown in Figure 5 does not include the form factor, but the Fullprof refinements shown in Figure 4 do.

An unusual feature of the parent compound which extends to the the weakly diluted variants is the presence of needle-like magnetic domains, manifested as the broadening of magnetic peaks which have large $\vec{Q}$ components in the ab plane. Figure 5 shows that the correlation length, and hence domain size, decreases with gallium content. Since magnetostriction has been proposed as an origin for the formation of antiferromagnetic domains[26,27], one might infer that the presence of smaller Ga ions at Fe sites creates strain or chemical pressure that locally increases the influence of magnetostriction, i.e., domain wall nucleation at impurities. However, as noted above, assuming a uniform distribution of Ga does not reproduce the inferred domain wall density. Some insight on the origin of the small domain size in the ab plane is provided by Figure 5b, which reveals that the correlation length and the helical winding length track each other for all measured

V. CONCLUSIONS

Our study of the magnetic dilution series $Fe_{3-x}Ga_xPO_4O_3$ reveals that the incommensurate magnetic structure present in the parent compound ($x = 0$) undergoes continuous changes with increasing x, until at high enough dilution ($x \sim 0.5$) a spin-glass-like state with no long range order forms. We find, by analyzing magnetic neutron powder diffraction patterns across the series, that the helical winding length and ab plane correlation length both decrease as x increases, but remain nearly equal to one another over the range $x = 0$ to 0.25. Based on numerical analysis of a Heisenberg exchange Hamiltonian with competing near neighbor (J_1) and next near neighbor (J_2) interactions, it is observed that the decreasing pitch length is consistent with a decreasing ratio of J_2/J_1, as expected from mean field considerations. Unexpectedly, the ab plane correlation length decreases in the same manner as the helical pitch length; the result is that despite the increased spacing in Q between satellite peaks for higher x, they still cannot be individually resolved. The coincidence of the two length scales suggests an intrinsic mechanism for the truncation of the the helical spin structure, rather than the nucleation of domain walls at impurities. These results further validate that magnetic frustration is responsible for the development of the helical magnetic structure in $Fe_3PO_4O_3$, while also providing clues as to the mechanism for the development of small needle-like domains of this structure. We anticipate that future studies of single crystal samples of $Fe_3PO_4O_3$ could elucidate the nature of this short range antiferromagnetic helical structure and its relation to topological spin textures.

VI. ACKNOWLEDGMENTS

Appendix A: Additional Information

Additional data from the neutron powder diffraction experiments are provided in this Appendix. The phase fractions of all crystalline phases detected in neutron powder diffraction are compiled in Table I. The raw neutron powder diffraction data at multiple temperatures are provided in Figure 7.

TABLE I. Phase fractions of primary and impurity phases detected by neutron powder diffraction at $T = 295$ K. All values in mol%.

Nominal comp.	$Fe_{3-x}Ga_xPO_7$	Fe_2O_3	$FePO_4$	$GaPO_4$
Fe_3PO_7	98(1)	0	2.0(3)	0
$Fe_{2.988}Ga_{0.012}PO_7$	95.9(6)	1.4(1)	2.7(1)	0
$Fe_{2.94}Ga_{0.06}PO_7$	97.2(3)	0.7(1)	2.1(2)	0
$Fe_{2.75}Ga_{0.25}PO_7$	93.9(5)	2.1(1)	4.01(2)	0
$Fe_{2.5}Ga_{0.5}PO_7$	93.5(4)	2.1(1)	4.4(1)	0
$Fe_2Ga_1PO_7$	90.9(5)	2.3(1)	0.3(1)	6.5(3)
$Fe_{1.5}Ga_{1.5}PO_7$	94.1(5)	0.6(1)	0	5.3(2)

* kate.ross@colostate.edu; Corresponding author

[1] A. Yoshimori, J. Phys. Soc. Jap. **14**, 807 (1959).

[2] T. A. Kaplan, Phys. Rev. **116**, 888 (1959).

[3] M. Itoh, I. Natori, S. Kubota, and K. Motoya, J. Phys. Soc. Jap. **63**, 1486 (1994).

[4] G. R. Blake, L. C. Chapon, P. G. Radaelli, S. Park, N. Hur, S.-W. Cheong, and J. Rodríguez-Carvajal, Phys. Rev. B **71**, 214402 (2005).

[5] L. Balents, Nature **464**, 199 (2010).

[6] T. Okubo, S. Chung, and H. Kawamura, Physical review letters **108**, 017206 (2012).

[7] J. Sampaio, V. Cros, S. Rohart, A. Thiaville, and A. Fert, Nature Nanotechnology **8**, 839 (2013).

[8] C. Pfleiderer, A. Rosch, A. Neubauer, R. Georgii, and P. Boni, Science **323**, 915 (2009).

[9] N. Nagaosa and Y. Tokura, Nature Nanotechnology **8**, 899 (2013).

[10] Y. Zhou and M. Ezawa, Nature Comm. **5**, 4652 (2014).

[11] X. Zhang, Y. Zhou, and M. Ezawa, Sci. Rep. **6**, 24795 (2016).

[12] K. A. Ross, M. M. Bordelon, G. Terho, and J. R. Neilson, Physical Review B **92**, 134419 (2015).

[13] J. Barker and O. A. Tretiakov, Physical Review Letters **116**, 147203 (2016).

[14] B. Göbel, A. Mook, J. Henk, and I. Mertig, Physical Review B **96**, 060406 (2017).

[15] G. Gavoille, C. Gleitzer, and G. J. Long, Revue de chimie minérale **24**, 42 (1987).

[16] A. Modaressi, A. Courtois, R. Gerardin, B. Malaman, and C. Gleitzer, J. Solid State Chem. **47**, 245 (1983).

[17] Q. Shi, L. Zhang, M. E. Schlesinger, J. Boerio-Goates, and B. F. Woodfield, J. Chem. Thermodyn. **62**, 86 (2013).

[18] S. Boudin and K.-H. Lii, Acta Crystallographica Section C: Crystal Structure Communications **54**, 5 (1998).

[19] V. O. Garlea, B. C. Chakoumakos, S. A. Moore, G. B. Taylor, T. Chae, R. G. Maples, R. A. Riedel, G. W. Lynn, and D. L. Selby, Applied Physics A **99**, 531 (2010).

[20] J. Rodríguez-Carvajal, Physica B **192**, 55 (1993).

[21] S. Toth and B. Lake, J. Phys.: Cond. Matt. **27**, 166002 (2015).

[22] P. Schiffer and I. Daruka, Physical Review B **56**, 13712 (1997).

[23] B. Martínez, F. Sandiumenge, A. Rouco, A. Labarta, J. Rodríguez-Carvajal, M. Tovar, M.T. Causa, S. Galí and X. Obradors, Phys. Rev. B **46**, 786 (1992).

[24] B. Fåk, R. A. Sadykov, J. Flouquet, and G. Lapertot, J. Phys.: Cond. Matt. **17**, 1635 (2005).

[25] C. Hammond and C. Hammond, *Basics of crystallography and diffraction*, Vol. 214 (Oxford, Oxford University Press, New York, 2001).

[26] A. Minakov, I. Shvets, and V. Veselago, Journal of Magnetism and Magnetic Materials **88**, 121 (1990).

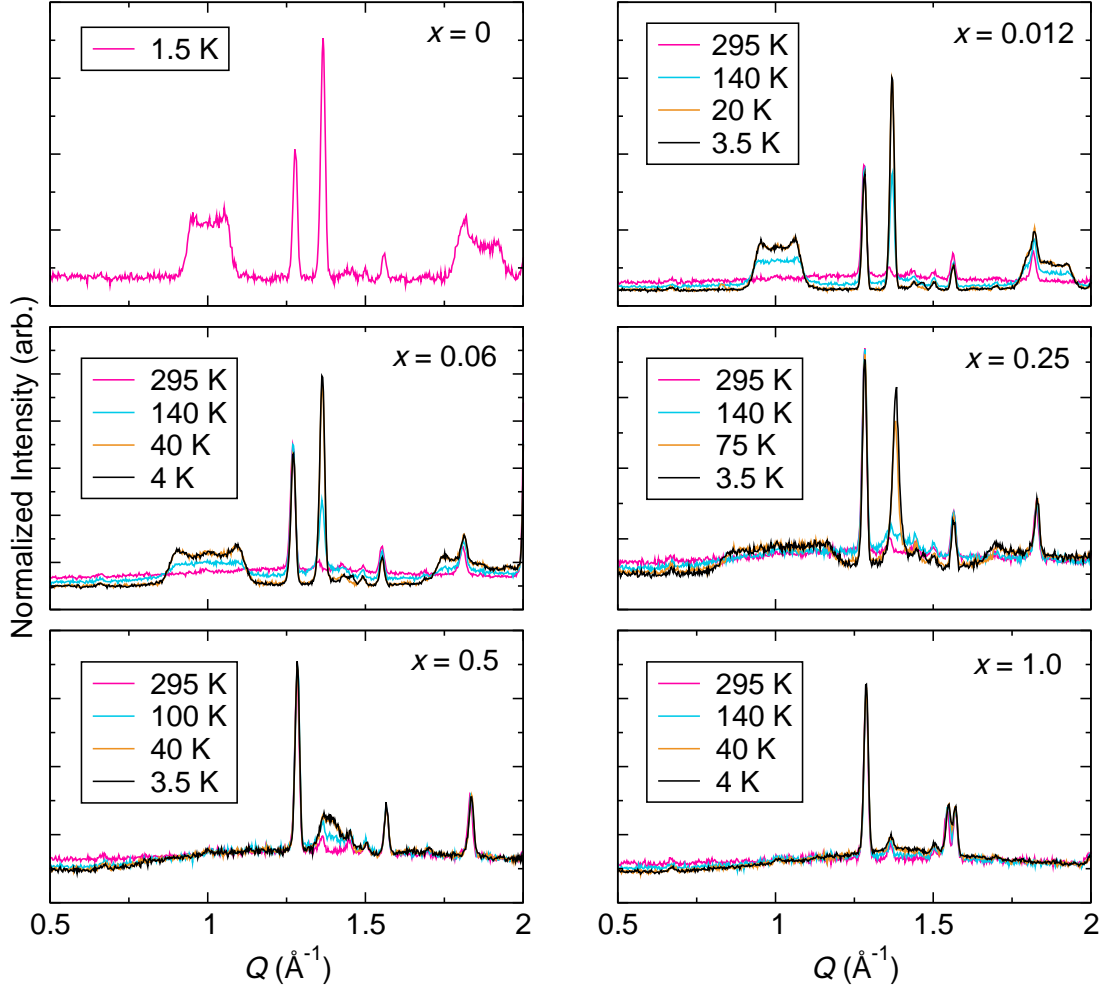[27] H. Gomonay and V. M. Loktev, J. Phys.: Cond. Matt. **14**, 3959 (2002).

FIG. 7. Raw data from neutron powder diffraction of $Fe_{3-x}Ga_xPO_4O_3$ at all temperatures and values of x. $FePO_4$ impurity peaks are denoted with black stars and $GaPO_4$ impurity peaks are denoted with blue addition signs.